A New Mechanism For Generating Type-III Radiation From The Sun

F.S. Mozer[1,2], O. Agapitov[1], S.D. Bale[1,2], K. Goetz[3], V. Krasnoselskikh[4], M. Pulupa[1], K. Sauer[5], and A. Voshchepinets[6]

1 Space Sciences Laboratory, University of California, Berkeley, California
2 Physics Department, University of California, Berkeley, California
3 University of Minnesota, Minneapolis, Minnesota
4 LPC2E, CNRS-University of Orléans-CNES, 45071, Orléans, France
5 Max-Planck Institute of Solar System Research, Göttingen, Germany
6 Uehgorod University, Ukraine

ABSTRACT

Because the conventional method of creating type-III radiation by coalescence of counter-propagating Langmuir waves has not been verified with in-situ data, Parker Solar Probe data was examined in search of such in-situ evidence, which was not found. Instead, a new mechanism for creating type-III radiation has been found as a result of observing slow Langmuir waves (~2200 km/sec) with electric fields as large as 300 mV/m during a developing type-III burst on March 21, 2023. Because of their slow phase velocities, these Langmuir waves had short wavelengths, several times the Debye length of 2.65 meters, and, as a result, $k\lambda_d \sim 0.93$. Such waves may be strongly damped to be replaced by new growing bursts of waves that create the characteristic Langmuir waveform that is composed of peaks and valleys of a few milliseconds' duration. The average electron current that produced these Langmuir waves is estimated from the Generalized Ohm's law to be ~15 microamps/m^2 and, from the strahl, 8 microamps/m^2. Peak currents were at least twice these averages. These Langmuir waves, acting as antennas, produced electrostatic harmonics having slow phase velocities (~2000 km/sec) at frequencies of $n\omega_p$, where $\omega_p = 2\pi*125$ kHz is the Langmuir wave frequency and n = 2, 3, 4, 5, 6, and 7. Such waves are not the type-III emission. As at least the first harmonic wave evolved through the huge density irregularities, its wave number decreased and it became the electromagnetic wave that was the type-III radiation.

I INTRODUCTION

The theory of type-III bursts was described by Ginsburg and Zhelezniakov [1958] who considered the two-stream instability of an electron beam which generates Langmuir (plasma) waves that are converted into electromagnetic emission by coalescence of two Langmuir waves. The theory has subsequently been discussed and refined by many authors (e.g. Sturrock 1964; Zheleznyakov & Zaitsev 1970; Smith 1970; Smith et al. 1976; Melrose 1980c; Goldman 1983; Dulk 1985; Melrose 1987). The two-step process, production of Langmuir waves, some of which interact with density irregularities to become backward waves that coalesce with the forward waves in a three-wave process that produces the electromagnetic

type-III radiation, is considered the basic mechanism. An additional mechanism, interactions of the plasma oscillations with ion sound waves to produce electromagnetic waves near the plasma frequency, has also been observed.

The first in-situ spectral observations of plasma waves in association with type-III emissions were made in 1976 [Gurnett and Anderson, 1976]. The simultaneous observation of Langmuir and electromagnetic waves was presented as strong evidence of the direct conversion of pairs of Langmuir waves into type-III waves, although the direct, in-situ, evidence of this interaction was not and has not been obtained.

II DATA

On March 21, 2023, the Parker Solar Probe was located about 45 solar radii from the Sun when it became embedded in the active type-III emission region illustrated in Figure 1a. Note the small colored lines under the emission (at the plasma frequency) which indicate times when large electric fields appeared in the radio frequency data. The type-III emission covered the frequency range from about 200 to 400 kHz at the time of about 26 bursts of high-rate data illustrated in Figure 1b. That the emission range covered more than just twice the plasma frequency has been noted earlier [Kellogg, 1980; Reiner and MacDowell, 2019; Jebaraj et al, 2023] and this aspect of the emission will be investigated below. The high frequency data bursts each consisted of ~15 milliseconds of electric and magnetic field measurements at a data rate of about 1.9 million samples/second [Bale et al, 2016].

The local plasma frequency, illustrated in Figure 1c, was determined as $8980n^{0.5}$, where n is the plasma density obtained from a least-squares fit of the spacecraft potential to the square root of the density obtained from the quasi-thermal noise measurement. By comparison of this frequency with the vertical lines beneath the type-III emission in Figure 1a, it is seen that the waves observed in the bursts were at or near the plasma frequency.

To interpret these observations in more detail, the largest amplitude burst event is further examined in Figures 2a through 2f. It is emphasized that the unusual properties of this event, discussed below, are typical of all Langmuir wave events observed on this day although this event had the largest electric field. Panels 2a and 2b give the two electric field components in the spacecraft X-Y plane, which show that the field was as large as 300 mV/m and it varied, as in typical Langmuir wave observations, on a millisecond time scale. Panel 2c gives the density fluctuations, $\Delta N/N$, whose magnitude was in agreement with that expected in a Langmuir wave. This is the first measurement of this relationship although it has been studied previously [Neugebauer, 1975; Kellogg et al, 1999]. Figure 2d presents the oblique angle between the Langmuir k-vector and the magnetic field in the X-Y plane. Because B_z was almost zero at this time, the error associated with ignoring the out-of-the-X-Y-plane components in this measurement is small. It shows that the waves were oblique to the magnetic field most of the time.

Panels 2e and 2f are the X and Y components of the electric field that are band pass filtered between 200 and 2000 Hz. They are related to the electron current by the Generalized Ohm's Law which is

$$\mathbf{E}+\mathbf{v}\times\mathbf{B} = \eta\mathbf{J} + \mathbf{J}\times\mathbf{B}/ne - \nabla\mathbf{P}/ne + (m_e/n^2)\partial\mathbf{J}\ \partial t \quad (1)$$

where
v = plasma velocity
η = anomalous resistivity
J = plasma current
n = plasma density
$\nabla\mathbf{P}$ = pressure gradient

For the corona, the scale of the terms on the right-hand side of Ohm's law is about 10^{-8}, 10^{-7}, 10^{-9}, and 10^{-10}, so the term of interest, $\mathbf{J}\times\mathbf{B}/ne$, after expansion, for B_x=-88 nT, B_y=48 nT, B_z=-3 nT becomes

$$neEX = -3J_y - 48J_z \quad (2)$$
$$neEY = -88J_z + 3J_x \quad (3)$$

where E_X and E_Y are given in Figures 2e and 2f. If J_z is comparable to J_x and J_y, equations (2) and (3) are approximately

$$J_z = -neE_X/48 = 0.5 \text{ microamps/m}^2 \quad (4)$$
$$J_z = -neE_Y/88 = 1.8 \text{ microamps/m}^2 \quad (5)$$

Because these two values of J_z differ by a factor of about four, J_z cannot be comparable in magnitude to J_x and J_y. Because $B_Z<B_X$ and $B_Z<B_Y$, one may assume that J_z is zero, for which equations (2) and (3) become two equations with two unknowns that yield time varying solutions for J_x and J_y whose average magnitudes are about

J_x = 14 microamps/m^2
J_y = 29 microamps/m^2

If J_z is small but not zero, J_x and J_y would be somewhat smaller. Thus, the typical value of the current is 15±10 microamps/m^2 and the peak current is about twice these values. These currents are comparable to the rough estimate of current obtained from the product of the ion density and temperature. It is noted that the currents, obtained from the fields of Figure 2e and 2f, oscillate during the same few millisecond intervals as do the electric fields of Figure 2a and 2b. This will be interpreted as decay of the wave because $k\lambda_d \sim 0.93$ where k is the Langmuir wave number and λ_d is the Debye length.

Figure 3a shows the electron velocity distribution function (vdf) during an 80 second interval surrounding the 15-millisecond large field event of Figure 2, using data obtained from on-board electron measurements [Whittlesey et al, 2020]. Because the time interval of this data collection is about 5000 times the duration of Figure

2 and because Langmuir waves appeared only a small fraction of this time (see Figure 1a), the vdf of Figure 3a is an average over an interval that is largely devoid of Langmuir waves. The strahl current obtained from this data, js=-1.6*10^(-19)*11*4386*10^9=-7.72 microamps/m^2, is consistent with but smaller than that estimated from the above equations. As noted, the peak current must have been at least a factor of two larger. Figure 3b presents the hodogram of the electric field in the X-Y plane. Because, as noted, B_Z~0, the hodogram illustrates the relationship between the electric field k-vector and the magnetic field (the green line in Figure 3b). From 3b it is seen that the electric field was generally parallel to the background magnetic field with deviations that are described in Figure 2d.

Figure 4 presents spectra of the electric filed (black), magnetic field (red) and density fluctuations for the Figure 2 event. All three had spectral peaks at the plasma frequency of 125 kHz, with the magnetic field peak presumed to result from interaction of the plasma oscillations with ion sound waves to produce Z-mode waves [Gurnett and Anderson, 1976; Hospodarsky and Gurnett, 1995]. At the seven harmonics of the Langmuir frequency of the large event, prominent electric fields were observed having no magnetic field components. Each of the spectral peaks consisted of a pair of closely spaced lines [Bale et al, 1996; Kellogg et al, 1999; Henri et al, 2009] which indicates that there are two sources that have been discussed in relation to the mechanism of current-driven waves [Sauer et al, 2017, 2019]. These electrostatic fields, must have been produced by antenna waves emanating from the Langmuir wave [Malaspina et al, 2012]. Because they are electrostatic, these harmonics cannot be the type-III emission.

The phase velocities of the waves are estimated from the data of Figure 5 that presents 100 microsecond views of the electric fields of Figure 2 at the plasma frequency (panels 5a, 5b, and 5c) and at twice the plasma frequency (panels 5d, 5e, and 5f). Panels 5c and 5f give the potentials of antenna one, V1, and the negative of the antenna two potential, -V2. At both the plasma frequency and its harmonic, these two potentials were offset in time relative to each other because of the time required for the waves at both frequencies to propagate from one antenna to the other. These propagation times depend on the phase velocity of the wave and the angle, A, between the propagation direction and the line from V1 to V2, because the distance that the wave traveled between the two antennas was 4*cos(A) meters. For both the Langmuir wave and its harmonic, the largest time delays between the peaks of V1 and -V2 were 1.8 microseconds when the angle, A, was close to zero. Thus, the phase velocities of both the Langmuir wave and its first harmonic were about 4e-3/1.8e-6 meters/second or 2220 km/sec. The higher harmonics were observed to have similar phase velocities. The hodogram of one period of the wave in Figure 5a is presented as the red curve in Figure 3b.

The distance between antenna V1 and antenna V2 was set to 4 meters when computing the phase velocity of the Langmuir wave. The geometry of the antennas and the spacecraft body are complex, so the exact value of this dimension is uncertain but the best estimate of this distance is 4±1 meters.

The fundamental wave with a frequency of 125 kHz and a phase velocity of 2220 km/sec has a wavelength that is 17.8 meters. From the electron core temperature of 23 eV and the plasma density of 181 cm^{-3}, both obtained from the vdf of Figure 3a, the Debye length was 2.65 meters. Thus, $k\lambda_d \sim 0.93$, and the Langmuir wave might be expected to decay rapidly. However, the amplitude of the wave at any time is determined by the balance between its source and loss. If the source was constant, the wave amplitude would be constant and determined by equating the source rate with the loss rate. If the source shut off abruptly, the wave amplitude would decrease at the decay rate. Thus, an upper limit to the decay rate may be obtained from the fastest decrease of the wave amplitude if such a decrease was due to the decrease in the source rate. The fastest decrease of the wave amplitude in Figure 2 is a few hundred microseconds. Thus, the unique shape of the Langmuir wave offers additional evidence that its decay rate is fast and that $k\lambda_d$ is the order of unity. The rapidly varying currents, whose proxies are the plots of Figures 2e and 2f, show that the Langmuir wave source varied rapidly, in support of the above analysis.

From the electron cyclotron frequency of 2750 Hz, the ratio of the cyclotron frequency to the plasma frequency was 0.022.

III DISCUSSION

There are only two wave modes in the frequency range above the plasma frequency, namely the slow extraordinary wave, SE, (sometimes called the Z-mode) and the ordinary, or O, electromagnetic wave. Because the phase velocities of the observed waves were much less than the speed of light, they are neither mode, but, instead, they are antenna generated waves. Conversion of these slow electrostatic waves into fast electromagnetic waves via propagation through an inhomogeneous plasma is a process that has been well-studied [Stix, 1965; Oyo, 1971; Melrose, 1980a; Melrose, 1981; Mjolhus et al, 1983; Morgan and Gurnett, 1990; Kalaee et al, 2009; Schleyer et al, 2013; Kim et al, 2013; Kalaee et al, 2016]. It is presumed that the electrostatic harmonics are converted to type-III emissions in this way.

The above data analysis shows that, for a large amplitude Langmuir wave event,

$$n\omega_p = \omega_n$$

and

$$n\mathbf{k_p} = \mathbf{k}_n$$

where n = 1, 2, 3, 4, 5, 6, or 7, ω_p and $\mathbf{k_p}$ are the frequency and wave number of the Langmuir wave, and ω_n and $\mathbf{k}_n$ are the frequency and wave number of the nth electrostatic wave. These results are consistent with

the Longmuir wave, acting as an antenna, generating the observed higher frequency electrostatic waves. Such electrostatic waves have the same range of frequencies as the classical type-III electromagnetic radiation but they have very short wavelengths and slow phase velocities, such that they cannot be the type-III emission. Theories of such waves, produced in density cavities [Ergun et al, 2008; Malaspina et al, 2012], do not apply to the present observations because density cavities were not present at times of any of the events discussed on the day of interest.

An unexpected result of the analysis is that $k\lambda_d \sim 0.93$, and the Langmuir wave might be expected to decay rapidly. However, the amplitude of the wave is determined by the balance between its source and loss. If the source was constant, the wave amplitude would be constant and determined by equating the source rate with the loss rate. Thus, without further knowledge about the source properties, one can neither confirm nor rule out a large decay rate for the Langmuir waves.

Previously observed electric fields have ranged from a few to about 100 millivolts/meter [Gurnett and Anderson, 1976; Graham and Cairns, 2012; Sauer et al, 2017]. This range is associated with the range of driving current densities in the plasma. The observed electric field of about 300 mV/m is a factor of three larger than the largest of any previously observed Langmuir waves [Malaspina et al 2010]. The explanation of this difference lies in the fact that the Langmuir waves have a wavelength of ~15 meters. This is longer than the three-meter Parker Solar Probe antenna but it is much shorter than the typical antennas that made the earlier measurements. An antenna that is longer than the wavelength of the wave it measures, under-estimates the amplitude of the true electric field because of the many wavelengths of the field that are inside the antenna. This antenna property explains why the largest earlier measurements produced smaller electric fields than observed in the current example.

The fact that $k\lambda_d \sim 0.93$ or, equivalently, that the core electron thermal velocity (2897 km/sec) was greater than the Langmuir wave phase velocity (2220 km/sec), presents a problem because Langmuir waves cannot be generated from an electron beam for such parameters. A possible resolution of this problem is that, in Figure 3, the core thermal electron temperature was determined over a time duration that was 5000 times longer than the duration of the wave of Figure 2 and this longer region was only partially filled with Langmuir waves. If the core electron temperature in the beam that produced the Langmuir waves had a smaller temperature than that in the surrounding region, $k\lambda_d$ would be smaller and the following theory would explain the Langmuir wave generation.

The interpretation of the measured electrostatic and electromagnetic fields at frequencies very close to the electron plasma frequency, ω_p, is based on the results of previous studies [Sauer and Sydora, 2015, 2016; Sauer et al, 2017, 2019] on the excitation of current-driven Langmuir oscillations with $\omega=\omega_e$ and $k=0$ by which, subsequently, a

parametric decay in Langmuir and ion-acoustic waves with finite wave number is triggered. It is assumed that the electron component is composed of two parts: a dominant population at rest and a minor component in relative motion, as seen in the core, halo and strahl of Figure 3. The mechanism of wave excitation does not take into account beam instabilities that may occur in an earlier phase of the interaction. The electron current resulting from the relative motion between the two electron components is crucial for triggering the Langmuir oscillations. A characteristic electron velocity distribution function of the solar wind is shown in Figure 6a together with the related dispersion of Langmuir waves in the wave number range up to $k\lambda_d=0.6$. As seen in Figure 6b, due to the occurrence of the electron-acoustic mode which is associated with the strahl, mode splitting takes place at the point where the Langmuir mode of the main population is crossed, that is at $k\lambda_d\sim0.3$. Correspondingly, the related phase velocity is $V_{ph}\sim3.5V_e$ (Figure 6b). Around this point the Langmuir/electron-acoustic mode is weakly damped (Figure 6c) and its frequency approaches the plasma frequency, ω_p, (see red points). As shown in earlier papers [Sauer and Sydora, 2015, 2016, Sauer et al, 2017, 2019], the current due to the strahl drives Langmuir oscillations at ω_e and simultaneously Langmuir/electron-acoustic waves are driven by parametric decay. Their wave length is given by that of the electron-acoustic mode at $\omega\sim\omega_e$, which in our case is $k\lambda_d\sim0.3$.

IV ACKNOWLEDGEMENTS

This work was supported by NASA contract NNN06AA01C. The authors acknowledge the extraordinary contributions of the Parker Solar Probe spacecraft engineering team at the Applied Physics Laboratory at Johns Hopkins University. The FIELDS experiment on the Parker Solar Probe was designed and developed under NASA contract NNN06AA01C. Our sincere thanks to J.W. Bonnell, M. Moncuquet, and P. Harvey for providing data analysis material and for managing the spacecraft commanding and data processing, which have become heavy loads thanks to the complexity of the instruments and the orbit.

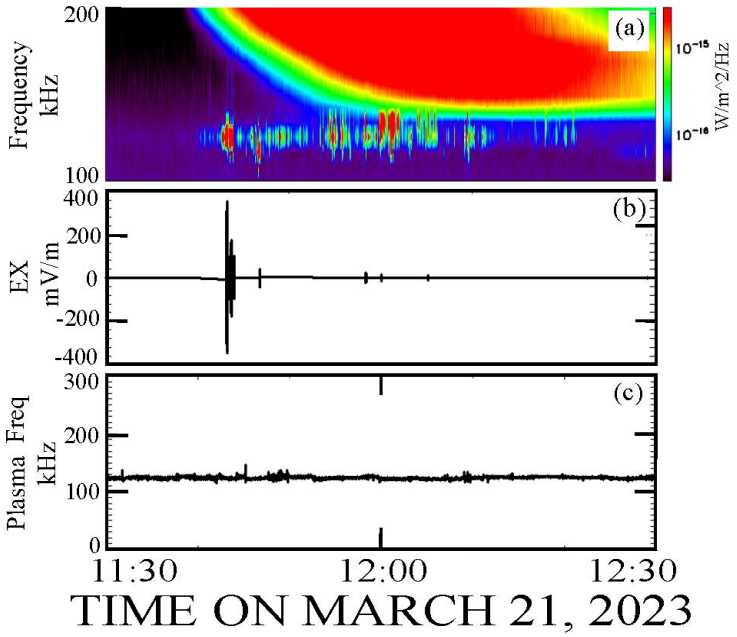

Figure 1. Overview of a type-III emission observed on March 21, 2023 (panel 1a) in which the spacecraft was embedded, showing bright lines below the emission due to large electric fields. From the plasma frequency of 125 kHz in Figure 1c, it is seen that these bright lines were due to waves at or near the plasma frequency. Note that these waves are present only part of the time. Figure 1b shows the times and electric field amplitudes of 26 data bursts taken for durations of about 15 milliseconds each at data rates in excess of one million samples/second.

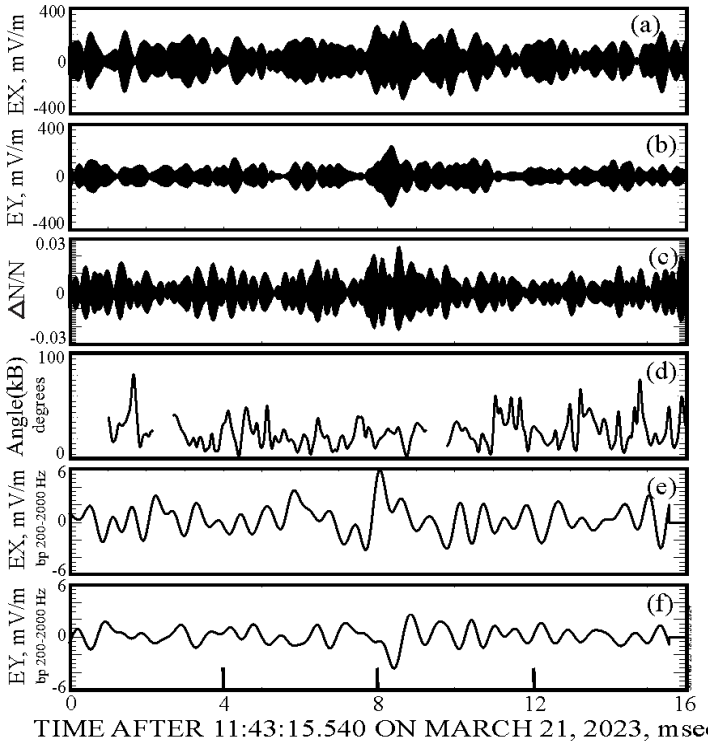

Figure 2. The largest amplitude data burst (panels 2a through 2f) observed during the type-III emission. Figures 2a and 2b give the X and Y components of the electric field in the spacecraft frame, with the X component being the surprisingly large 300 mV/m. Figure 1c gives the density fluctuations that are expected to accompany a Langmuir wave. Figure 2d presents the angle in the X-Y plane between the background magnetic field and the electric field wave vector. Figures 2e and 2f give the electric field after being band pass filtered from 200 to 2000 Hz. This data is associated with the electron beam current through the Generalized Ohm's Law.

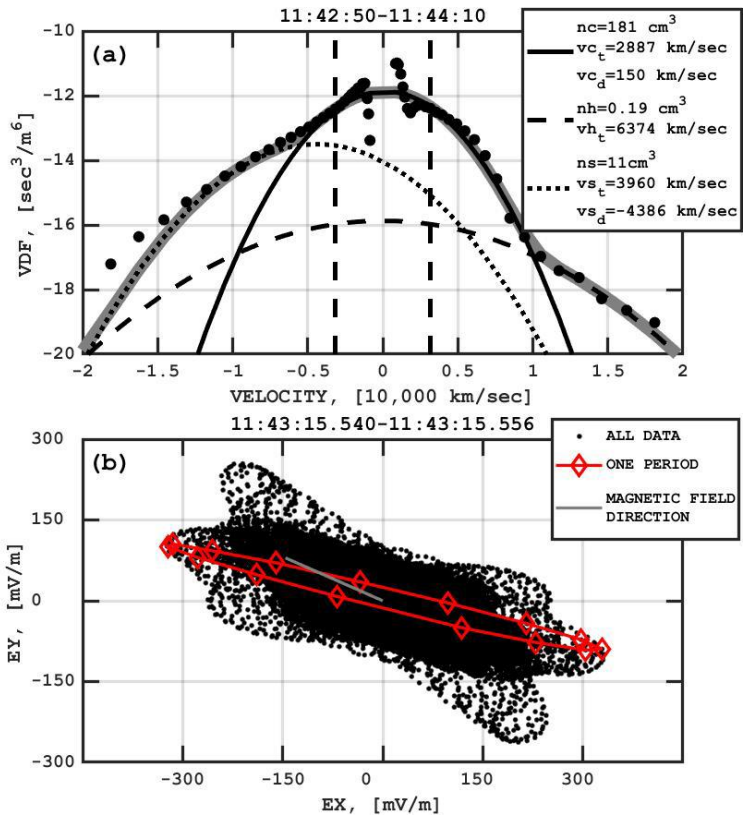

Figure 3. Panel 3a gives the electron velocity distribution function during an 80 second interval surrounding the 15-millisecond large Langmuir wave. It describes the core, halo and strahl distributions and it shows that the average core electron density and thermal velocity were 181 cm^{-3} and 2887 km/sec. Panel 3b gives the hodogram of the electric field during this event. The hodogram is in the X-Y plane but, because $B_Z \sim 0$, it describes the relationship between the electric field and the magnetic field direction, which is the green line. It is seen that the electric field is generally parallel to the magnetic field with significant deviations that are described in Figure 2d. The red curve in Figure 3b represents one period of the wave at the time of the data in Figure 5.

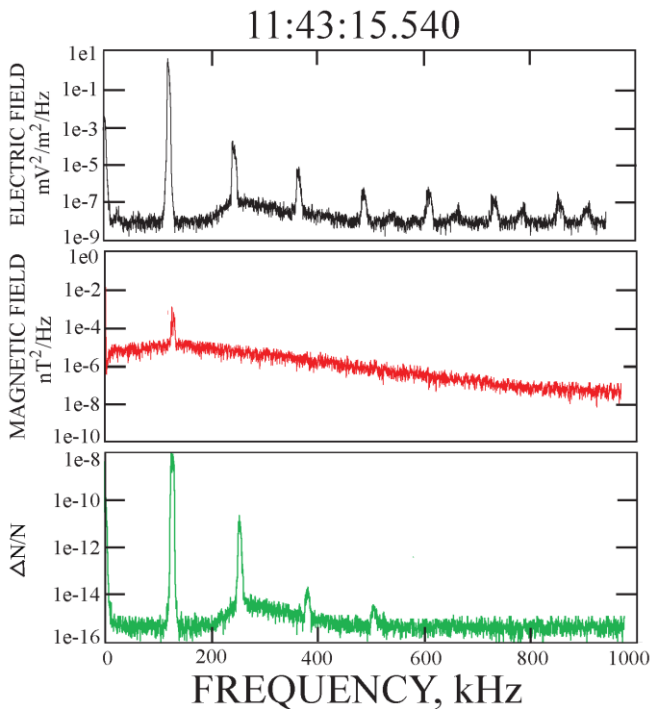

Figure 4. Spectra of the electric field, the magnetic field and the density fluctuations observed during the intense burst at 11:43:15.540. The lowest frequency wave, at 125 kHz, is the Langmuir wave which has both a magnetic and density fluctuation component while the harmonics of the Langmuir wave are electrostatic since they had no magnetic component. Six electric field harmonics of the intense burst are observed.

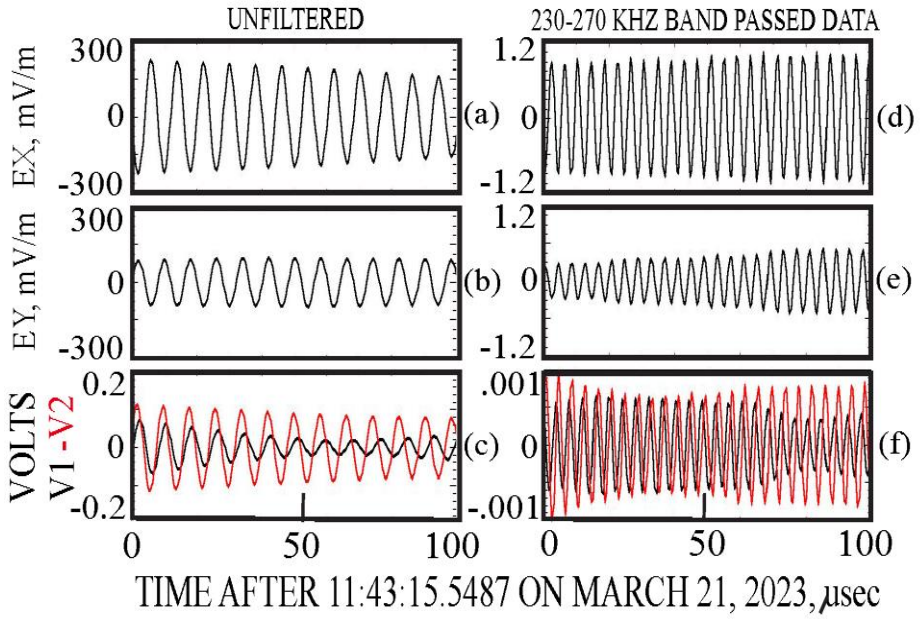

Figure 5. One hundred millisecond expanded views of the electric field at the Langmuir frequency (panels 5a and 5b) and at the first harmonic (panels 5d, and 5e). Panels 5c and 5f give the potential of antenna 1, V1, and the negative of the potential of antenna 2, -V2. There is a time lag between these two measurements at both frequencies, such that the time required for the wave to cross the antenna system was about 1.8 microseconds. Thus, both waves had slow phase velocities and neither wave (nor those at the higher harmonics) could be the 0-mode type III radiation.

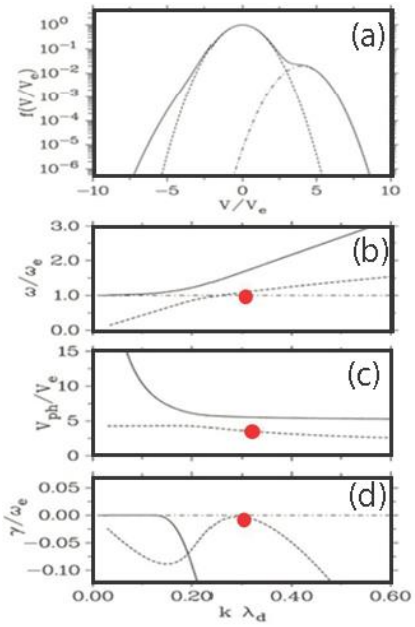

Figure 6. a) Electron velocity distribution function (EVDF) of the solar wind consisting of core, halo and strahl and the associated dispersion of the Langmuir/electron-acoustic mode. b) frequency ω/ω_e, c) phase velocity Vph/Ve (Ve: thermal core velocity) and d) damping rate γ/ω_e.

REFERENCES

Bale, S. D., Burgess, D., Kellogg, P. J., Goetz, K., Howard, R. L., & Monson, S. J., 1996. GRL, 23, 109–112. https://doi.org/10.1029/95GL03595

Bale, S.D., Kellogg, P.J., Goetz, K., and Monson, S.J., 1998, GRL, 25, NO. 1, 9-12

Bale, S. D., Goetz, K., Harvey, P. R., et al. 2016, SSRv, 204, 49

Dulk, G. A. 1985, ARA&A, 23, 169

Ergun, R.E., Malaspina, D.M., Cairns, I,H, et al, 2008, *PRL* **101**

Ginzburg, V.L. and Zheleznyakov, V.V., Sov. Astron. AJ 2, 653 (1958)

Goldman, M. V., Reiter, G.F. and Nicholson, D.R., 1980, Phys. Fluids, 23, 388 – 401.

Graham, B., and Cairns, I.H., 2012, JGR: SPACE PHYSICS, 118, 3968–3984, doi:10.1002/jgra.50402

Gurnett, D. A. and Anderson, R. R. 1976. Science. 194 (4270): 1159–1162

Henri, P., Briand, C., Mangeney, A., Bale, S. D., Califano, F., Goetz, K., & Kaiser, M., 2009, JGR, 114(A13), 3103. https://doi.org/10.1029/2008JA013738

Hospodarsky, G.B. and Gurnett, D.A., 1995, GRL, **22**, NO. 10, 1161-1164

Jebaraj,I.C., Krasnosalskikh, V., Pulupa, M., Magdalenic, J., and Bale, S.D. , 2023, Ap.J., **955:L20** https://doi.org/10.3847/2041-8213/acf85

Kalaee, M.J., Ono, T. Katoh, Y, Lizima, M., and Nishimura, Y., 2009, Earth Planets Space, **61**, 1243–1254

Kalaee, M.J., Katoh, Y., 2016, *Phys. Plasmas*, **23**, 072119, https://doi.org/10.1063/1.4958945

Kellogg, P.J., 1980, Ap.J., 236, 696-700

Kellogg, P.J., Goetz, K, and Monson, S.J., 1999, JGR, 104, A8, 17,069-17,078

Kim, E.H., Cairns, I.H. and Johnson, J.R., 2013, *Phys. Plasmas*, **20**, 122103

Larosa, A., Dudok de Wit, T., Krasnoselskikh1, V., Bale, S.D., Agapitov, O., Bonnell, J.W., et al, 2022, Ap.J., 927:95 (8pp) https://doi.org/10.3847/1538-4357/ac4e85

Malaspina, D.M., Cairns, I.H., and Ergun, R.E. 2010, JGR, 115, A01101, doi:10.1029/2009JA014609

Malaspina, D.M., Cairns, I.H., and Ergun, R.E. 2012, Ap.J., **755:45**, doi:10.1088/0004-637X/755/1/45

Malaspina, D. M., Graham, D.B., Ergun, R.E.,and Cairns, I.H., 2013, JGR, Space Physics, **118**, 6880–6888, doi:10.1002/2013JA019309

Melrose, D. B. 1980, Space Sci. Rev., 26, 3

Melrose, D.B., 1980a, Aust. J. Phys, 33,661

Melrose, D.B., 1981, Journal of Geophysical Research: Space Physics, **86**, Issue A1 / p. 30-36, https:/ /doi.org/10.1029/JA086iA01p00030

Melrose, D. B. 1987, Sol. Phys., 111, 89

Mjolhus, E., 1983, Journal of Plasma Phy, **30** Issue 2 pp. 179 - 192 DOI: https://doi.org/10.1017/S0022377800001

Morgan, D.D., and Gurnett, D.A., 1990, *Radio Sci.*,**25**(6), 1321–1339, doi:https://doi.org/10.1029/RS025i006p01321

Neugebauer, M., 1976, Geophys. Res., 81, 2447, 19

Oyo, H., 1971, Radio Science, **6**, Issue 12, pp. 1131-1141 DOI:10.1029/RS006i012p01131

Papadopoulos, K., Freund, H.P. 1978, Geophys. Res. Lett., 5, 881 – 884

Reiner, M.J. and MacDowall, R.J., 2019, Solar Phys (2019) 294:91 https://doi.org/10.1007/s11207-019-1476-9

Sauer, K., and Sydora, R., 2015, JGR, Space Physics, 120, doi:10.1002/2014JA020409.

Sauer, K., and Sydora, R., 2016, Geophys. Res. Lett., 43, doi:10.1002/2016GL069872.

Sauer, K., Malaspina, D.M., Pulupa, M. and Salem, C.S., 2017, J. Geophys. Res. Space Physics, 122, 7005–7020, doi:10.1002/2017JA024258

Sauer, K., Baumgärtel, K., Sydora, R., and Winterhalter, D. 2019, JGR, Space Physics, 124, 68–89. https://doi.org/10.1029/2018JA025887

Schleyer; F., Cairns, I.H. and Kim, E.-H. 2013, *Phys. Plasmas* **20**, 032101, https://doi.org/10.1063/1.4793726

Smith, D. F. 1970, Sol. Phys., 15, 202

Smith, R. A., Goldstein, M. L., and Papadopoulos, K. 1976, Sol. Phys., 46, 515

Stix, T.H. ,1965, *Phys. Rev. Lett.*, **15**, 23

Sturrock, P. A. 1964, NASA Special Publication, 50, 357

Whittlesey, P.L., Berthomier, M., Larson, D.E., Case, A.W., Kasper, J.C., et al, 2020, Ap.J., 246, https://doi.org/10.3847/1538-4365/ab7370

Zheleznyakov, V. V., & Zaitsev, V. V. 1970, Soviet Ast., 14, 47